AGU ADVANCING EARTH AND SPACE SCIENCES

JGR Space Physics

RESEARCH ARTICLE
10.1029/2024JA033118

Resonant Scattering of Sub-keV Electrons by Beam-Driven Electron Cyclotron Harmonic Waves

Xu Zhang[1], Anton Artemyev[1], Vassilis Angelopoulos[1], Xiao-Jia Zhang[2], Qianli Ma[3,4], Xin An[1], and Ying-dong Jia[1]

[1]Department of Earth, Planetary, and Space Sciences, University of California, Los Angeles, CA, USA, [2]Department of Physics, University of Texas at Dallas, Richardson, TX, USA, [3]Department of Atmospheric and Oceanic Sciences, University of California, Los Angeles, CA, USA, [4]Center for Space Physics, Boston University, Boston, MA, USA

Key Points:

- We revise the equation to calculate the bounce-averaged diffusion coefficients of beam-driven Electron Cyclotron Harmonic (ECH) waves
- Beam-driven ECH waves resonate with lower-energy electrons compared to previously studied loss cone driven ECH waves
- Beam-driven ECH waves effectively scatter ionospheric electron outflows out of the loss cone, trapping them within the magnetosphere

Supporting Information:

Supporting Information may be found in the online version of this article.

Correspondence to:

X.-J. Zhang,
xuzhang@igpp.ucla.edu

Citation:

Zhang, X., Artemyev, A., Angelopoulos, V., Zhang, X.-J., Ma, Q., An, X., & Jia, Y.-d. (2025). Resonant scattering of sub-keV electrons by beam-driven electron cyclotron harmonic waves. *Journal of Geophysical Research: Space Physics*, *130*, e2024JA033118. https://doi.org/10.1029/2024JA033118

Received 30 JUL 2024
Accepted 19 DEC 2024

Abstract Electron cyclotron harmonic waves (ECH) play a key role in scattering and precipitation of plasma sheet electrons. Previous analysis on the resonant interaction between ECH waves and electrons assumed that these waves are generated by a loss cone distribution and propagate nearly perpendicular (~88°) to the background magnetic field. Recent spacecraft observations, however, have demonstrated that such waves can also be generated by low energy electron beams and propagate at moderately oblique angles (~70°). To quantify the effects of this newly observed ECH wave mode on electron dynamics in Earth's magnetosphere, we use quasi-linear theory to calculate the associated electron pitch angle diffusion coefficient. Utilizing THEMIS spacecraft measurements, we analyze in detail a few representative events of beam-driven ECH waves in the plasma sheet and the outer radiation belt. Based on the observed wave properties and the hot plasma dispersion relation of these waves, we calculate their bounce-averaged pitch angle, momentum and mixed diffusion coefficients. We find that these waves most efficiently scatter low-energy electrons (10–500 eV) toward larger pitch angles, on time scales of 10^2 to 10^3 seconds. In contrast, loss-cone-driven ECH waves most efficiently scatter higher-energy electrons (500 eV–5 keV) toward lower pitch-angles. Importantly, beam-driven ECH waves can effectively scatter ionospheric electron outflows out of the loss cone near the magnetic equator. As a result, these outflows become trapped in the magnetosphere, forming a near-field-aligned anisotropic electron population. Our work highlights the importance of ECH waves, particularly beam-driven modes, in regulating magnetosphere-ionosphere particle and energy coupling.

1. Introduction

Magntosphere-ionosphere coupling involving mass and energy exchange between ionospheric and magnetospheric plasma, substantially influences the dynamics of both regions (Khazanov et al., 2014; Lysak, 1990; Strangeway et al., 2005). While electrons can precipitate into the ionosphere along magnetic field lines (Frank & Ackerson, 1971; Newell et al., 2009; Ni et al., 2016; Thorne et al., 2010), low-earth-orbit (LEO) spacecraft observations have revealed upward-streaming electrons escaping from the ionosphere toward the magnetosphere (Artemyev, Zhang, et al., 2020; Carlson et al., 1998; Cattell et al., 2004; Elphic et al., 2000). These escaping electrons can be accelerated upward by quasi-static electric field structures frequently observed in the upper ionosphere (Ergun et al., 1998, 2001; Mozer et al., 1977). They can also be formed via secondary electrons produced by energetic electron precipitation from the magnetosphere (Artemyev, Zhang, et al., 2020; Khazanov et al., 2017, 2019). Electron outflows often coincide with downward field-aligned currents and are crucial elements of the global field-aligned current systems (Carlson et al., 1998; Iijima & Potemra, 1976, 1978). Assuming conservation of the first adiabatic invariant, electron outflows should be confined within the loss cones as they reach the magnetic equator and bounce along the magnetic field lines between hemispheres (Marshall & Bortnik, 2018; Mourenas et al., 2021). Near-equatorial spacecraft measurements, however, have frequently detected a field-aligned anisotropic electron population at sub-keV energies in the inner magnetosphere and in the plasma sheet (Artemyev et al., 2014; Chappell et al., 2008; Denton et al., 2017; Walsh et al., 2011). Because these field-aligned anisotropic electrons likely originate from the ionosphere (Artemyev et al., 2014; Walsh et al., 2013; Zheng et al., 2012), their presence suggests that ionospheric electron outflows can be scattered out of the loss cone through non-adiabatic process near the magnetic equator and become trapped in the magnetosphere (Abel et al., 2002a, 2002b). This pitch angle scattering is often attributed to resonant interactions with plasma waves (Kennel & Petschek, 1966; Schulz & Lanzerotti, 1974; Zhang et al., 2018). It is, therefore, natural for us to investigate the plasma waves responsible for trapping electron outflows in the magnetosphere. The formation of

this anisotropic electron population through wave-particle interactions in the magnetosphere is important because it contributes to the total electron current in the central plasma sheet (e.g., Artemyev, Angelopoulos, et al., 2020; Kamaletdinov et al., 2020, and references therein).

Various plasma waves in Earth's magnetosphere can resonantly interact with electrons. A few of them can pitch-angle scatter electrons in the sub-keV energy range out of the loss cone, and thus are potential candidates for trapping electron outflows into the magnetosphere. Upper-band chorus waves can scatter electrons from hundreds of eV to a few keV through cyclotron resonance (Meredith et al., 2009; Ni et al., 2008), while highly oblique chorus waves (in both the lower and upper band) resonate with sub-keV electrons through Landau resonance (Artemyev et al., 2016; Mourenas et al., 2012; Zhang et al., 2022a, 2022b). Time domain structures, solitary waves formed in the nonlinear stage of beam-driven instabilities (e.g., An et al., 2021), also scatter sub-keV electrons (Shen et al., 2020, 2021; Vasko et al., 2017). A recent study (Horne, 2015) demonstrates that electron cyclotron harmonic (ECH) waves driven by a loss cone distribution can scatter and energize electron outflows in the sub-keV energy range and trap them in the magnetosphere. ECH waves are electrostatic emissions with wave power between nf_{ce} and $(n+1)f_{ce}$, where f_{ce} is the electron cyclotron frequency and $n = 1, 2, 3\ldots$ (Fredricks & Scarf, 1973; Kennel et al., 1970; Meredith et al., 2009). ECH waves in Earth's magnetosphere have been observed predominantly in the night and dawn sectors, that is, at locations coinciding with drift paths of energetic electrons injected from the nightside plasma sheet (Meredith et al., 2009; Ni et al., 2017; Ni, Thorne, Liang, et al., 2011; Roeder & Koons, 1989). Because ECH waves are electrostatic waves with very small group velocities, they are often confined near the magnetic equator within a few degrees of magnetic latitude (Gough et al., 1979; Meredith et al., 2009; Paranicas et al., 1992; Zhang et al., 2014). Recent study have shown that ECH waves are also observed in the day sector not only near the equator but also at high latitudes (Yu et al., 2023, 2024). ECH waves have received substantial attention in the past few decades because of their important role in scattering energetic electrons into the loss cone and driving the diffuse aurora (Belmont et al., 1983; Horne et al., 2003; Horne & Thorne, 2000; Lou et al., 2018; Ni, Thorne, Horne, et al., 2011; Zhang et al., 2013). Although Horne (2015) demonstrated that ECH waves can scatter electrons from tens of eV to a few hundred eV very effectively through cyclotron resonance, it is more common for ECH waves to resonate with electrons at higher energies from a few hundred eV to a few keV and drive diffuse aurora precipitation (Horne & Thorne, 2000; Ni et al., 2016; Ni, Liang, et al., 2012). The contribution of ECH waves to diffuse aurora precipitation has also been investigated for decades (Belmont et al., 1983; Horne & Thorne, 2000; Lyons, 1984; Ni, Thorne, Horne, et al., 2011). Thorne et al. (2010) demonstrated that ECH waves are less effective than chorus waves in driving diffuse aurora at $L < 8R_E$. At larger distances, chorus wave intensities drop, and ECH waves dominate the plasma sheet electron losses (Ni, Liang, et al., 2012). Zhang et al. (2015) quantified the role of ECH waves in diffuse aurora precipitation more systematically: They compared the energy flux of precipitating electrons due to quasi-linear pitch angle scattering by ECH waves with the energy flux of diffuse aurora electron precipitation from the OVATION PRIME model (Newell et al., 2009). Their results demonstrated that ECH waves are the dominant driver for plasma sheet electron scattering and diffuse aurora precipitation at $L > 8R_E$.

Previous quantification of electron scattering driven by ECH waves assumed that these waves were driven by loss cone instability of energetic electrons at a few keV (Ashour-Abdalla et al., 1979; Ashour-Abdalla & Kennel, 1978; Fredricks, 1971; Karpman et al., 1975; Young et al., 1973). These loss-cone-driven ECH waves propagate nearly perpendicular to the ambient magnetic field, with wave normal angles $\theta(\vec{B},\vec{k}) \approx 88^\circ \sim 89^\circ$ (Ni, Thorne, Horne, et al., 2011; X. Liu et al., 2018). However, a recent study that included a number of us has revealed another significant population of ECH waves characterized by substantial field-aligned electric field fluctuations and moderately oblique propagation directions at $\theta(\vec{B},\vec{k}) \approx 70^\circ$ (Zhang, Angelopoulos, Artemyev, Zhang, & Liu, 2021). These moderately oblique ECH waves are driven by field-aligned electron beams at tens of eV to a few hundred eV (Zhang, Angelopoulos, Artemyev, & Zhang, 2021). Because wave normal angle is a key parameter determining the quasi-linear diffusion coefficients of ECH waves and the resultant diffusive electron scattering, beam-driven ECH waves interact with electrons quite distinctly compared with loss-cone-driven ECH waves: Loss-cone-driven ECH waves, characterized by their nearly transverse propagation, can scatter electrons at hundreds of eV to a few keV into the loss cone through cyclotron resonance (Belmont et al., 1983; Fontaine & Blanc, 1983; Horne & Thorne, 2000). In contrast, beam-driven ECH waves, with non-negligible parallel electric field fluctuations, not only interact with electrons through cyclotron resonance, but can also exchange momentum with electrons in the parallel direction through Landau resonance. Particle-in-cell simulations in Zhang

et al. (2024a, 2024b) demonstrated that beam-driven ECH waves can accelerate cold electrons at a few eV in both perpendicular and parallel directions through cyclotron and Landau resonances. They can also thermalize electron beams at tens of eV to a few hundred eV and scatter them further in velocity space through cyclotron resonance. However, there has been a lack of quantitative assessment of diffusive scattering of plasma sheet electrons by beam-driven ECH waves. Such analysis requires re-evaluating the quasi-linear diffusion coefficients of ECH waves by taking into account the effects of wave propagation. It is, therefore, the major objective of this study to quantify the contribution of beam-driven ECH waves to the diffusive scattering of plasma sheet electrons. By incorporating moderately oblique ECH waves into existing models of magnetospheric electron scattering, our study aims to improve our understanding of these plasma waves' role in influencing the mass and energy exchange in the coupled magnetosphere-ionosphere system.

Here we first analyze a representative event of beam-driven ECH waves observed by the Time History of Events and Macroscale Interactions during Substorms (THEMIS) mission (Angelopoulos, 2008; Sibeck & Angelopoulos, 2008). We then quantitatively evaluate the effects of these waves on plasma sheet electron scattering using quasi-linear theory. In Section 2, we explain our methodology for calculating the bounce-averaged diffusion coefficients of beam-driven ECH waves. In Section 3, we present an event of beam-driven ECH waves and analyze the associated diffusion coefficients. In Section 4, for comparison, we examine a representative event encompassing loss-cone-driven ECH waves and their diffusion coefficients. Section 5 is our summary and discussion.

2. Data and Methodology

2.1. Spacecraft Measurements

The THEMIS mission consists of five identically instrumented spacecraft (TH-A through TH-E) that were launched in 2007 (Angelopoulos, 2008). Two probes (TH-B and TH-C) arrived in lunar orbit in 2011, becoming the ARTEMIS (Acceleration, Reconnection, Turbulence and Electrodynamics of the Moon's Interaction with the Sun) mission (Angelopoulos, 2011). THEMIS's fluxgate magnetometer (FGM) (Auster et al., 2008) measures the direct-current magnetic field and its low frequency fluctuations (<64 Hz), and the search coil magnetometer (SCM) (Roux et al., 2008) measures the high frequency magnetic field (a few Hz up to 4 kHz). The Electric Field Instrument (EFI) (Bonnell et al., 2008) measures the low and high frequency electric field (<8 kHz). We will use waveform electric field data to analyze the properties of ECH waves observed. THEMIS Filter Bank (FBK) and Fast Fourier Transform (FFT) data products (Cully et al., 2008) are wave power spectra of electric and magnetic fields processed on board the spacecraft. We will also use data from the electrostatic analyzer (ESA) (McFadden et al., 2008) that measures <30keV particles to investigate the electron distribution functions during time intervals of ECH wave observations.

2.2. Theoretical Model

Based on theoretical work by Lyons (1974), the pitch angle diffusion coefficient of ECH waves is:

$$D_{\alpha\alpha} = \sum_{N=-\infty}^{+\infty} \int k_\perp dk_\perp \left[\Psi_{N,k} \left(\frac{N\Omega_{ce}/\omega_k - \sin^2\alpha}{\sin\alpha\cos\alpha} \right)^2 \right]_{k_\parallel = k_{\parallel,res}} \tag{1}$$

with

$$\Psi_{N,k} = \frac{1}{4\pi} \frac{e^2}{m_e^2} \frac{|E_k|^2}{V} \left(\frac{\omega_k}{|k|} \right)^2 \frac{J_N^2(k_\perp v_\perp/\Omega_{ce})}{v^4 \left(v_\parallel - \partial\omega_k/\partial k_\parallel \right)} \tag{2}$$

where $D_{\alpha\alpha}$ is the local pitch angle diffusion coefficient in units of s^{-1}, N is the resonance harmonic number obtained from the resonance condition,

$$\omega - k_\parallel v_\parallel = N\Omega_{ce} \tag{3}$$

Here, $k_\perp$ and $k_\parallel$ are wave vectors perpendicular and parallel to the background magnetic field, Ω_{ce} is the absolute value of electron cyclotron frequency, α is the local electron pitch angle, $k_{\parallel,res}$ is the parallel wave vector obtained from the resonance condition in Equation 3, e is the elementary charge, m_e is the electron mass, E_k is the electric field amplitude in wave number space, V is the plasma volume, and J_N is the Bessel function of the first kind of order N. Assuming the wave electric field has the form (Horne & Thorne, 2000):

$$|E_k|^2 = Ak_\perp^2 \exp\left[-\left(\frac{k_\perp}{k_{\perp,0}}\right)^2\right] \cdot\left\{\exp\left[-\left(\frac{k_\parallel - k_{\parallel,0}}{\Delta k_\parallel}\right)^2\right] + \exp\left[-\left(\frac{k_\parallel + k_{\parallel,0}}{\Delta k_\parallel}\right)^2\right]\right\} \tag{4}$$

with

$$A = \frac{4\pi^{3/2}}{k_{\perp,0}^4 \Delta k_\parallel} V|E_w|^2 \tag{5}$$

we can follow Horne and Thorne (2000) to obtain the pitch angle diffusion coefficient of ECH waves. When integrating Equation 1 in the perpendicular wave vector $dk_\perp$ direction, Horne and Thorne (2000) assumed wave normal angles of ECH waves close to 90° and approximated k with $k_\perp$. Therefore Horne and Thorne (2000) have

$$\begin{aligned}&\int_0^\infty k_\perp \frac{k_\perp^2}{k^2} J_N^2(k_\perp v_\perp/\Omega_{ce}) \exp\left[-\left(\frac{k_\perp}{k_{\perp,0}}\right)^2\right] dk_\perp \\ &= \int_0^\infty k_\perp J_N^2(k_\perp v_\perp/\Omega_{ce}) \exp\left[-\left(\frac{k_\perp}{k_{\perp,0}}\right)^2\right] dk_\perp \\ &= \frac{1}{2}k_{\perp,0}^2 \exp(-\lambda) In(\lambda)\end{aligned} \tag{6}$$

where $\lambda = \frac{1}{2}k_{\perp,0}^2 v_\perp^2/\Omega_{ce}^2$ and $In(\lambda)$ is the modified Bessel function. The assumption that $k^2 \approx k_\perp^2$, however, is not valid for moderately oblique ECH waves with the wave normal angles $\theta \ll 90°$. For such waves we modify Equation 6 as:

$$\begin{aligned}&\int_0^\infty k_\perp \frac{k_\perp^2}{k^2} J_N^2(k_\perp v_\perp/\Omega_{ce}) \exp\left[-\left(\frac{k_\perp}{k_{\perp,0}}\right)^2\right] dk_\perp \\ &= \int_0^\infty k_\perp \sin^2(\theta_k) J_N^2(k_\perp v_\perp/\Omega_{ce}) \exp\left[-\left(\frac{k_\perp}{k_{\perp,0}}\right)^2\right] dk_\perp \\ &\approx \frac{1}{2}k_{\perp,0}^2 \sin^2\theta \exp(-\lambda) In(\lambda)\end{aligned} \tag{7}$$

Thus, accounting for the wave normal angle θ of ECH waves, the local pitch angle diffusion coefficient becomes:

$$\begin{aligned}D_{\alpha\alpha} = &\frac{\pi^{1/2}}{2}\frac{e^2}{m_e^2}\frac{|E_w|^2}{k_{\perp,0}^2 \Delta k_\parallel}\frac{1}{v^5 \cos\alpha}\sin^2\theta \\ &\cdot \sum_{N=-\infty}^{+\infty}\left(\frac{N\Omega_{ce} - \omega_k \sin^2\alpha}{\sin\alpha\cos\alpha}\right)^2 \exp(-\lambda) In(\lambda) \\ &\cdot\left\{\exp\left[-(\zeta_N^-)^2\right] + \exp\left[-(\zeta_N^+)^2\right]\right\},\end{aligned} \tag{8}$$

where

$$\zeta_N^{\pm} = \frac{(\omega_k - N\Omega_{ce})}{\Delta k_{\|} v \cos\alpha} \pm \frac{k_{\|,0}}{\Delta k_{\|}}. \tag{9}$$

The local mixed diffusion coefficient $D_{\alpha p}$ and momentum diffusion coefficient D_{pp} are (Albert, 2007; Glauert & Horne, 2005):

$$\begin{aligned} D_{\alpha p} &= D_{\alpha\alpha}\left[\frac{\sin\alpha\cos\alpha}{N\Omega_{ce}/\omega_k - \sin^2\alpha}\right] \\ D_{pp} &= D_{\alpha\alpha}\left[\frac{\sin\alpha\cos\alpha}{N\Omega_{ce}/\omega_k - \sin^2\alpha}\right]^2 \end{aligned} \tag{10}$$

To calculate the bounce-averaged diffusion coefficients of ECH waves, we need to make an assumption about the magnetic field configuration. ECH waves are confined to the equator within a few degrees of magnetic latitude. Previous studies have shown minimal differences in bounce-averaged diffusion coefficients of ECH waves in dipole versus more realistic magnetic field configurations (Ni, Thorne, & Ma, 2012; Q. Ma et al., 2012). Therefore, in the following section we use a dipole magnetic field configuration due to its simplicity. The bounce-averaged diffusion coefficients of ECH waves are (Glauert & Horne, 2005; Summers et al., 2007; Q. Ma et al., 2016):

$$\begin{aligned} \langle D_{\alpha\alpha}\rangle &= \frac{1}{S(\alpha_{eq})}\int_0^{\lambda_m} D_{\alpha\alpha}(\alpha)\frac{\cos\alpha\cos^7\lambda}{\cos^2\alpha_{eq}}d\lambda \\ \langle D_{\alpha p}\rangle &= \frac{1}{S(\alpha_{eq})}\int_0^{\lambda_m} D_{\alpha p}(\alpha)\frac{\sin\alpha\cos^7\lambda}{\sin\alpha_{eq}\cos\alpha_{eq}}d\lambda \\ \langle D_{pp}\rangle &= \frac{1}{S(\alpha_{eq})}\int_0^{\lambda_m} D_{pp}(\alpha)\frac{\sin^2\alpha\cos^7\lambda}{\sin^2\alpha_{eq}\cos\alpha}d\lambda \end{aligned} \tag{11}$$

Here, α is the local pitch angle, α_{eq} is the equatorial pitch angle, λ is the magnetic latitude, and λ_m is the lower value between the maximum latitude where waves occur and the mirroring latitude of electrons. Because ECH waves are confined near the magnetic equator (Meredith et al., 2009; Ni, Thorne, Liang, et al., 2011), the maximum latitude of waves is chosen to be 3° or the magnetic latitude where ECH waves reflect. We will use Equation 11 to calculate the bounce-averaged pitch angle, mixed, and momentum diffusion coefficients for both beam-driven and loss-cone-driven ECH waves in the following sections.

3. Beam-Driven ECH Waves

Figure 1 presents an event of beam-driven ECH waves observed by THEMIS-A at a radial distance of $11R_E$ in the nightside plasma sheet, within Dipolarizing Flux Bundles (DFBs). DFBs are transient phenomena in Earth's magnetotail characterized by a sharp increase in the south-north component of the magnetic field and are often accompanied by fast plasma sheet flows (Angelopoulos et al., 1992; Nakamura et al., 2002; Runov et al., 2009; J. Liu, Angelopoulos, Runov, & Zhou, 2013; J. Liu, Angelopoulos, Zhou, et al., 2013). ECH waves in Earth's magnetotail have often been correlated with electron injections and DFBs (Liang et al., 2011; Zhang & Angelopoulos, 2014; Zhang et al., 2014). Figure 1a shows DFBs arriving at THEMIS-A around 04:41 UT. ECH waves are observed prior to and after the DFBs' arrival, as shown in Figure 1c. These waves have power in the first, second and third harmonic frequency bands, with the strongest power in the first harmonic. To identify the free energy source for ECH wave generation, we examine electron flux anisotropy at different energies. Figure 1b reveals enhanced field-aligned flux anisotropy in the energy range from tens of eV to a few hundred eV. The correlation between this field-aligned anisotropic electron population and ECH wave power suggests that ECH waves may be generated by field-aligned electron beams in the sub-thermal energy range (Zhang, Angelopoulos, Artemyev, Zhang, & Liu, 2021). We zoom into the time interval from 04:44:43 UT to 04:44:51 UT, when wave burst data is available. Figure 1d shows electric field waveform data in the field-aligned coordinate system, where Z_{FAC} is along the background magnetic field direction, ϕ_{SM} is the azimuthal direction in Solar Magnetospheric coordinate, X_{FAC} is defined as $X_{FAC} = -\phi_{SM} \times Z_{FAC}$, and Y_{FAC} completes the right-handed orthogonal

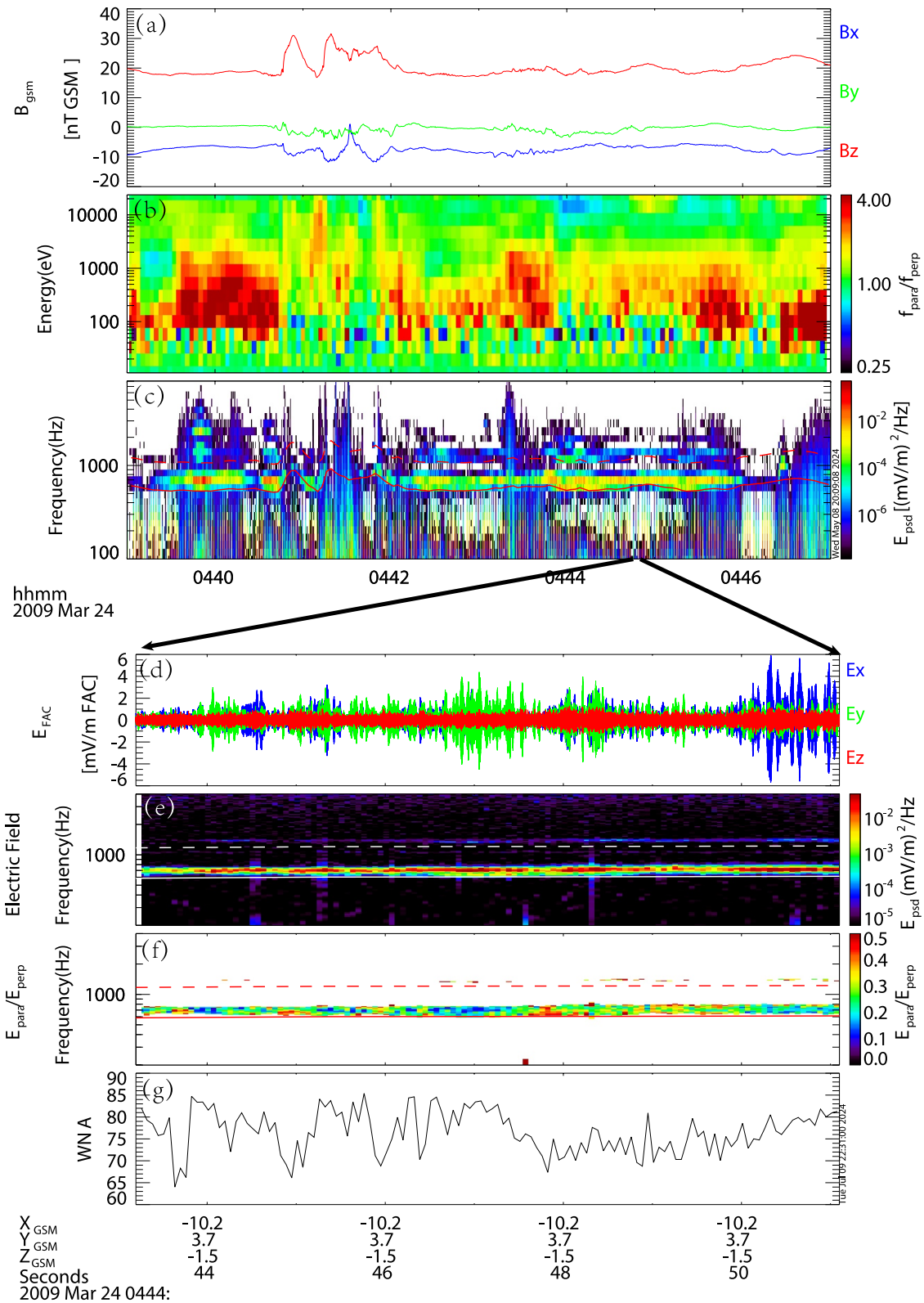

Figure 1.

coordinate system. The ECH wave frequency is $f = 709$ Hz, with the local electron cyclotron frequency $f_{ce} = 606$ Hz. The small magnitudes of $B_{X,GSM}$ and $B_{Y,GSM}$ in Figure 1a suggest that the satellite is located very close to the central plasma sheet. Therefore, we use the local electron cyclotron frequency measured by the spacecraft to approximate the electron cyclotron frequency at the wave generation region. The average wave electric field amplitude is 1.55 mV/m, with its parallel component being 0.34 mV/m. Figure 1f illustrates the square root of the ratio between parallel and perpendicular electric field power spectral densities. The non-negligible parallel electric field fluctuations are typical of beam-driven ECH waves (Zhang, Angelopoulos, Artemyev, Zhang, & Liu, 2021; Zhang et al., 2022a, 2022b). The absence of magnetic field fluctuations (not shown) confirms that ECH waves are electrostatic with longitudinal oscillations $\vec{k} \| \overrightarrow{E_w}$. As a result, the wave normal angle of ECH waves can be calculated from the ratio of parallel to total wave electric fields $\cos\theta(\vec{B},\vec{k}) = E_{\|}/E_{total}$. The average wave normal angle of ECH waves is $\theta(\vec{B},\vec{k}) = 77°$, as shown in Figure 1g; that is, these are moderately oblique ECH waves.

To calculate the bounce-averaged diffusion coefficients of beam-driven ECH waves, we need their dispersion relation. This can be obtained by fitting the electron distribution functions in Figure 2, observed concurrently with ECH waves. It is evident that there are counter-streaming electron beams in the directions parallel and antiparallel to the background magnetic field, with beam energies around 100 ~ 300 eV. We fit the observed electron distribution functions with drifting-Maxwellian distributions:

$$f(v_\perp, v_\|) = \sum_\alpha \frac{n_\alpha}{\pi^{3/2} v_{th\perp,\alpha}^2 v_{th\|,\alpha}} \exp\left(-\frac{v_\| - v_{d,\alpha}}{v_{th\|,\alpha}}\right)^2 \exp\left(-\frac{v_\perp^2}{v_{th\perp,\alpha}^2}\right), \tag{12}$$

where n_α is the number density of species α, $v_{th\perp}$ and $v_{th\|}$ are thermal velocities in the perpendicular and parallel directions, and v_d is the drift velocity in the parallel direction. Table 1 lists the fitting results of the observed electron distribution function. Using these fitted parameters as inputs, we solve the hot plasma dispersion relation of beam-driven ECH waves using the HOTRAY code (Horne, 1989). The most unstable mode, with growth rate $\gamma/\omega_{ce} = 0.0014$, occurs at wave number $k = 0.0018\mathrm{m}^{-1}$, wave frequency $f/f_{ce} = 1.08$, and wave normal angle $\theta = 71°$. Both Landau resonance and cyclotron resonance with the electron beam contribute to the generation of these waves. The wave frequency and the wave normal angle from linear instability analysis agree well with spacecraft observations in Figure 1. We use the observed wave parameters with $E_w = 1.55$ mV/m, $\theta = 77°$, $f/f_{ce} = 1.17$, $k_{\perp,0} = 0.0048\mathrm{m}^{-1}$ and $k_{\|,0} = 0.0011\mathrm{m}^{-1}$ to calculate the local pitch angle diffusion coefficient in Equation 8. $k_{\perp,0}$ and $k_{\|,0}$ are determined by solving the hot plasma dispersion relation $D(\omega,k,\theta) = 0$ at the observed wave frequency and normal angle. The angular width of the wave electric field is $\Delta\theta = 2.5°$ and the spectral width is $\Delta k_\| = k_{\perp,0}/\tan(\theta - \Delta\theta) - k_{\|,0}$.

We use the local diffusion coefficients from Equation 8 and Equation 10 to calculate the bounce-averaged diffusion coefficients in a dipole magnetic field configuration. We use the HOTRAY ray-tracing code to trace the propagation of beam-driven ECH waves and obtain wave parameters distributed along the magnetic field line. Detailed ray-tracing results can be found in Figure S1 in the Supporting Information S1. The maximum allowable latitude for waves in this integration is chosen to be 3°, because ECH waves are confined near the magnetic equator (Meredith et al., 2009; Ni, Thorne, Liang, et al., 2011) (The waves typically reflect before reaching that latitude.) Figure 3 illustrates the bounce-averaged pitch angle diffusion coefficients of beam-driven ECH waves at different energies. At 10 eV and 100 eV, $\langle D_{\alpha\alpha}\rangle$ is very large in a wide range of pitch angles $\alpha = 0° \sim 80°$. The scattering of low energy electrons is mainly due to cyclotron resonance at $N = 1$ and $N = 2$, where N is the resonance harmonic number in Equation 3. Landau resonance at $N = 0$ can also scatter electrons at 100 eV at intermediate pitch angles. Beam-driven ECH waves can be very effective in scattering low-energy electron beams

Figure 1. An event of beam-driven ECH waves observed by the THEMIS-A spacecraft in the plasma sheet. (a) Magnetic field in GSM coordinate system; (b) Ratio between the parallel electron phase space density and perpendicular electron phase space density as a function of electron energy and time. Red indicates field-aligned flux anisotropy and blue is perpendicular flux anisotropy; (c) Electric field dynamic power spectrum. Solid red line is f_{ce} and dashed red line is $2f_{ce}$; (d) Electric field waveform data in field-aligned coordinate system after high-pass filtering above 100 Hz; (e) Electric field dynamic power spectrum. Solid white line is f_{ce} and dashed white line is $2f_{ce}$; (f) Square root of the ratio between the parallel electric field power spectral density and the perpendicular power spectral density. Solid red line is f_{ce} and dashed red line is $2f_{ce}$. Only data points when the total power spectral density is larger than $10^{-4}(mV/m)^2/Hz$ are plotted; (g) Wave normal angle of ECH waves.

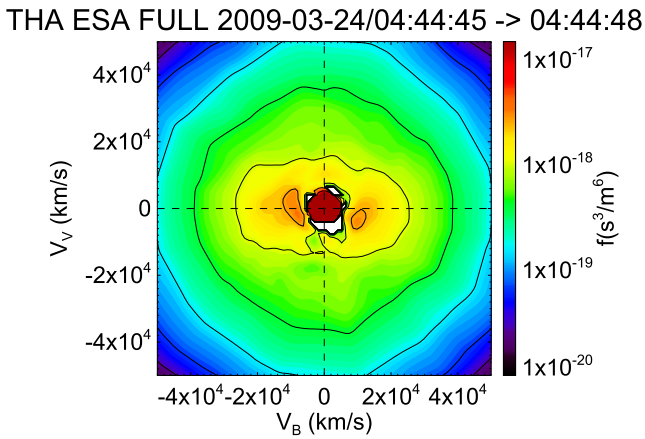

Figure 2. Electron phase space density observed by the THEMIS-A ESA instrument in one satellite spin period (~3*s*) from 04:44:45 UT to 04:44:48 UT. The horizontal axis is electron velocity in the direction parallel to the background magnetic field. The vertical axis is perpendicular electron velocity in the plane defined by the magnetic field direction and the electron bulk velocity direction. Red circle in the middle of the plot is due to photo-electron emissions. Only bins above the one-count-level threshold are plotted.

in the energy range of tens of eV to a few hundred eV out of the loss cone, that is, toward larger pitch angles, thus magnetically trapping the field-aligned electrons within the magnetosphere. Such scattering process occurs on time scales around $10^2 \sim 10^3$ seconds. We modeled the evolution of the observed electron distribution function during the interaction with beam-driven ECH waves using 2-D bounce-averaged Fokker-Planck equation (Ni, Thorne, & Ma, 2012; Tao et al., 2011; Xiao et al., 2009; Zhang et al., 2013). Results in Figure S9 in the Supporting Information S1 further demonstrate that low energy electron beams can be thermalized on time scales around $10^2 \sim 10^3$ seconds.

Bounce-averaged pitch angle diffusion coefficients of beam-driven ECH waves at energies of 500 eV and 2 keV are illustrated in Figures 3c and 3d. In contrast to loss-cone-driven ECH waves which scatter the plasma sheet electrons through cyclotron resonances with $N = 1$ and $N = 2$ (Horne & Thorne, 2000), beam-driven ECH waves scatter plasma sheet electrons primarily through higher-order cyclotron resonances with $N \geq 3$ and $N \leq -2$. At 500 eV, bounce-averaged diffusion coefficient at the edge of the loss cone $\langle D_{\alpha\alpha} \rangle_{\alpha=\alpha_{LC}}$ is larger than the strong diffusion limit D_{SD}, defined as:

$$D_{\mathrm{SD}} = 4\alpha_{LC}^2/\tau_{bounce} \quad (13)$$

where α_{LC} is the equatorial loss cone, τ_{bounce} is the electron bounce period calculated using Tsyganenko 96 magnetic field model (Tsyganenko, 1995). $\langle D_{\alpha\alpha} \rangle_{\alpha=\alpha_{LC}}$ at energy of 2 keV is also comparable to the strong diffusion limit. Our results suggest that beam-driven ECH waves can effectively scatter plasma sheet electrons into the loss cone, driving diffuse aurora precipitation. Figure 4 illustrates bounce-averaged pitch angle, momentum and mixed diffusion coefficients of beam-driven ECH waves. In the energy range of a few eV to a few hundred eV, both the pitch angle and momentum diffusion coefficients are considerably large in a wide range of electron pitch angles. Cold electrons at a few eV can be energized by beam-driven ECH waves. More importantly, electron beams at tens of eV to a few hundred eV, likely of ionospheric origin, can be thermalized and scattered toward higher pitch angles out of the loss cone through resonant interaction with beam-driven ECH waves. The interaction between beam-driven ECH waves and sub-keV electrons is consistent with the evolution of the electron distribution functions as shown in our previous PIC simulations(Zhang et al., 2024a, 2024b). At higher energies of a few hundred eV to a few keV, beam-driven ECH waves can efficiently fill the loss cone through resonant scattering of plasma sheet electrons.

The beam-driven ECH wave event of Figure 1 examined above was observed at $L = 11$ and $MLT = 22.7$, in Earth's plasma sheet, where such waves are typically observed. However, beam-driven ECH waves have also been observed in other regions of Earth's magnetosphere. We thus also investigated and presented in the Supporting Information S1 section a detailed analysis of typical beam-driven ECH wave events at the dawn sector with $L = 7.8$, $MLT = 5.9$ in Figures S4 and S5 in Supporting Information S1 and in the outer radiation belt with $L = 5.8$, $MLT = 21$ in Figures S2 and S3 in Supporting Information S1. We show that in these events too, the waves can very effectively scatter ionospheric electron outflows in the sub-keV energy range out of the loss cone toward higher pitch angles, thereby trapping them in the magnetosphere.

Table 1
The Parameters for the Electron Distribution Functions Fitted From Figure 2

	$n(cm^{-3})$	$T_{\parallel}(eV)$	$T_{\perp}/T_{\parallel}$	v_{drift}/v_{th}
Component 1	0.154	2,974	1.43	0
Component 2	0.112	5,088	0.59	0
Component 3	9.37×10^{-4}	8.7	22.66	5.17
Component 4	2.87×10^{-3}	84.2	2.29	2.98
Component 5	1.18×10^{-3}	8.15	12.21	−4.93
Component 6	4.25×10^{-3}	123.9	1.87	−2.53
Component 7	2×10^{-3}	0.1	1	0

4. Loss-Cone-Driven ECH Waves

To compare beam-driven ECH waves, that propagate at moderately oblique wave normal angles discussed previously (in Section 3) with classical loss cone driven ECH waves, we present here an event of loss-cone-driven ECH waves with wave normal angles close to 90°. Figure 5 shows such an event observed by THEMIS-E near the magnetic equator in the plasma sheet at $L = 10$, $MLT = 0$. The small magnitudes of $B_{X,GSM}$ and $B_{Y,GSM}$ suggest that the spacecraft was located very close to the equatorial plane at the time.

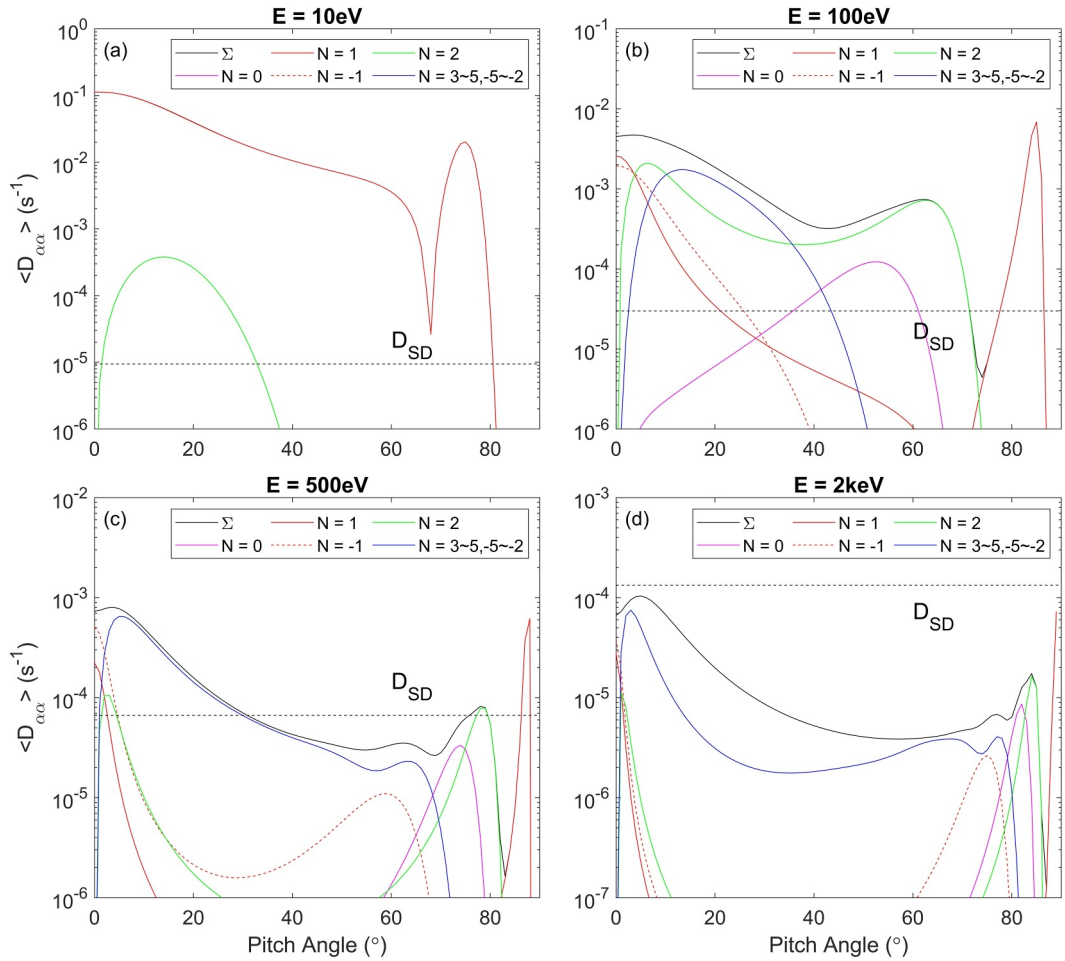

Figure 3. Bounce-averaged pitch angle diffusion coefficient of ECH waves as a function of electron pitch angle at different energies. Horizontal black dashed lines are strong diffusion limits. Black solid curve is diffusion coefficient calculated from the sum of resonance harmonic numbers N from −50 to 50. Red line is calculated from $N = 1$. Green line is calculated from $N = 2$. Magenta line is from Landau resonance when $N = 0$. Red dashed line is from $N = -1$. Blue line is from higher order cyclotron resonances when $N = 3 \sim 5$ and $N = -2 \sim -5$. (a) Bounce-averaged pitch angle diffusion coefficient at $E = 10eV$; (b) $E = 100eV$; (c) $E = 500eV$; (d) $E = 2keV$. The black solid curve nearly overlaps with the red line in Figure 3a.

Electron measurements show isotropic flux distribution in the sub-keV energy range. We zoom into the time interval when wave burst data is available, from 03:14:53 UT to 03:14:58 UT. ECH waves with power in their first harmonic frequency band, as well as higher harmonic bands, are evident in Figure 5c. We analyze only the properties of the first harmonic band and use it to calculate ECH diffusion coefficients because the wave power is strongest in that band. The average electric field wave amplitude is 7.53 mV/m and the average wave frequency is $f = 990$ Hz with $f/f_{ce} = 1.4$. We calculate the wave normal angles of ECH waves from the ratio between parallel and perpendicular electric field amplitudes. The averaged wave normal angle of ECH waves is $\theta = 88°$, suggesting that the observed ECH waves are likely driven unstable by loss cone distributions. The observed electron distribution function (see Figure S6 in the Supporting Information S1) further confirms the absence of electron beams streaming in parallel or antiparallel directions. We fit the observed electron distribution function with subtracted bi-Maxwellians (Ashour-Abdalla et al., 1979; Ashour-Abdalla & Kennel, 1978):

$$f(v_\perp, v_\parallel) = \sum_\alpha \frac{n_\alpha}{\pi^{3/2} v_{th\perp}^2 v_{th\parallel}} \exp\left(-\frac{v_\parallel - v_d}{v_{th\parallel}}\right)^2 \left[\Delta \exp\left(-\frac{v_\perp^2}{v_{th\perp}^2}\right) + \frac{1-\Delta}{1-\beta}\left(\exp\left(-\frac{v_\perp^2}{v_{th\perp}^2}\right) - \exp\left(-\frac{v_\perp^2}{\beta v_{th\perp}^2}\right)\right)\right]. \quad (14)$$

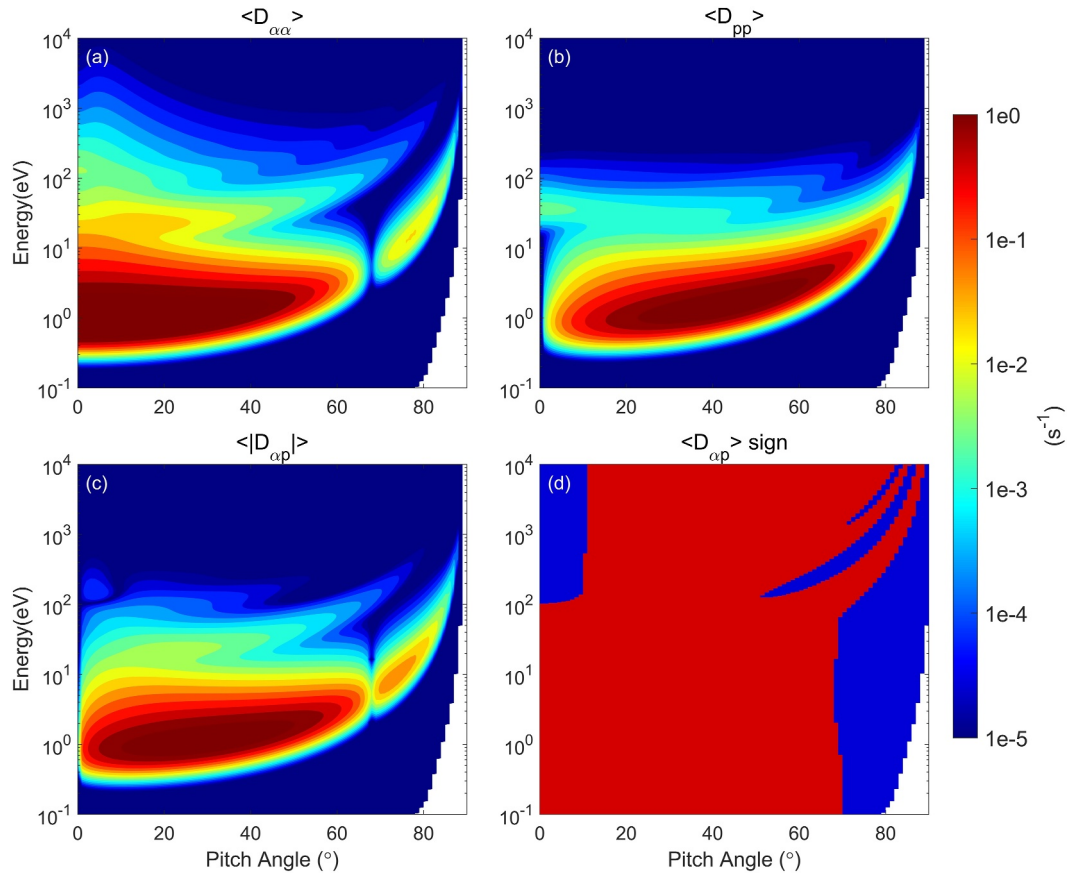

Figure 4. (a) Bounce-averaged pitch angle diffusion coefficient of beam-driven ECH waves as a function of electron energy and electron pitch angle; (b) Bounce-averaged momentum diffusion coefficient; (c) Bounce-averaged mixed diffusion coefficient; (d) The sign of mixed diffusion coefficient. Red is positive sign and blue is negative sign.

Here, Δ and β are two loss cone parameters representing the width and the depth of the loss cone, respectively. $\Delta = 1$ means no loss cone. We use the fitted distribution function (see Table S1 in the Supporting Information S1) as input parameters to the HOTRAY code to calculate the hot plasma dispersion relation of loss-cone-driven ECH waves. At the observed wave frequency $f/f_{ce} = 1.4$ and wave normal angle $\theta = 88°$, the wave number k is calculated to be 0.0026m^{-1}, and the growth rate $\gamma/\omega_{ce} = 4 \times 10^{-3}$. To calculate the bounce-averaged diffusion coefficients of loss-cone-driven ECH waves, we use the HOTRAY ray-tracing code to evaluate wave parameters along the magnetic field line (see Figure S7 in the Supporting Information S1). The maximum latitude λ_m in Equation 11 is chosen to be $\lambda_m = 1.7°$ where ECH waves reflect. The angular width $\Delta\theta$ of ECH waves is 2° and gradually decreases with latitude (Ni, Thorne, Horne, et al., 2011). Figure 6 presents the bounce-averaged pitch angle, momentum and mixed diffusion coefficients of the loss-cone-driven ECH waves. These waves can effectively scatter plasma sheet electrons in the energy range from a few hundred eV to a few keV into the loss cone, resulting in diffuse aurora precipitation. Pitch angle diffusion coefficients at the edge of the loss cone $\alpha_{LC} = 1.4°$ at energies of 500 eV, 1 keV, 5 keV are $\langle D_{\alpha\alpha}|_{E=500eV}\rangle = 1.96 \times 10^{-2}s^{-1}$, $\langle D_{\alpha\alpha}|_{E=1keV}\rangle = 1.33 \times 10^{-2}s^{-1}$, $\langle D_{\alpha\alpha}|_{E=5keV}\rangle = 1.8 \times 10^{-3}s^{-1}$ respectively. The strong diffusion limits at these energies are $\langle D_{\text{SD}}|_{E=500eV}\rangle = 1.03 \times 10^{-4}s^{-1}$, $\langle D_{\text{SD}}|_{E=1keV}\rangle = 1.46 \times 10^{-4}s^{-1}$, $\langle D_{\text{SD}}|_{E=5keV}\rangle = 3.25 \times 10^{-4}s^{-1}$ respectively. Loss-cone-driven ECH waves, therefore, can fill the loss cone of these electrons within a quarter of their bounce periods. We model the evolution of the observed electron distribution function using 2-D bounce-averaged Fokker-Planck equation. Our results demonstrate that loss-cone-driven ECH waves can effectively scatter plasma sheet electrons into the loss cone, leading to the formation of pancake distributions (see Figure S10 in the Supporting Information S1). Both loss-cone-driven and beam-driven ECH waves can scatter plasma sheet electrons at hundreds of eV to a few keV and drive diffuse aurora

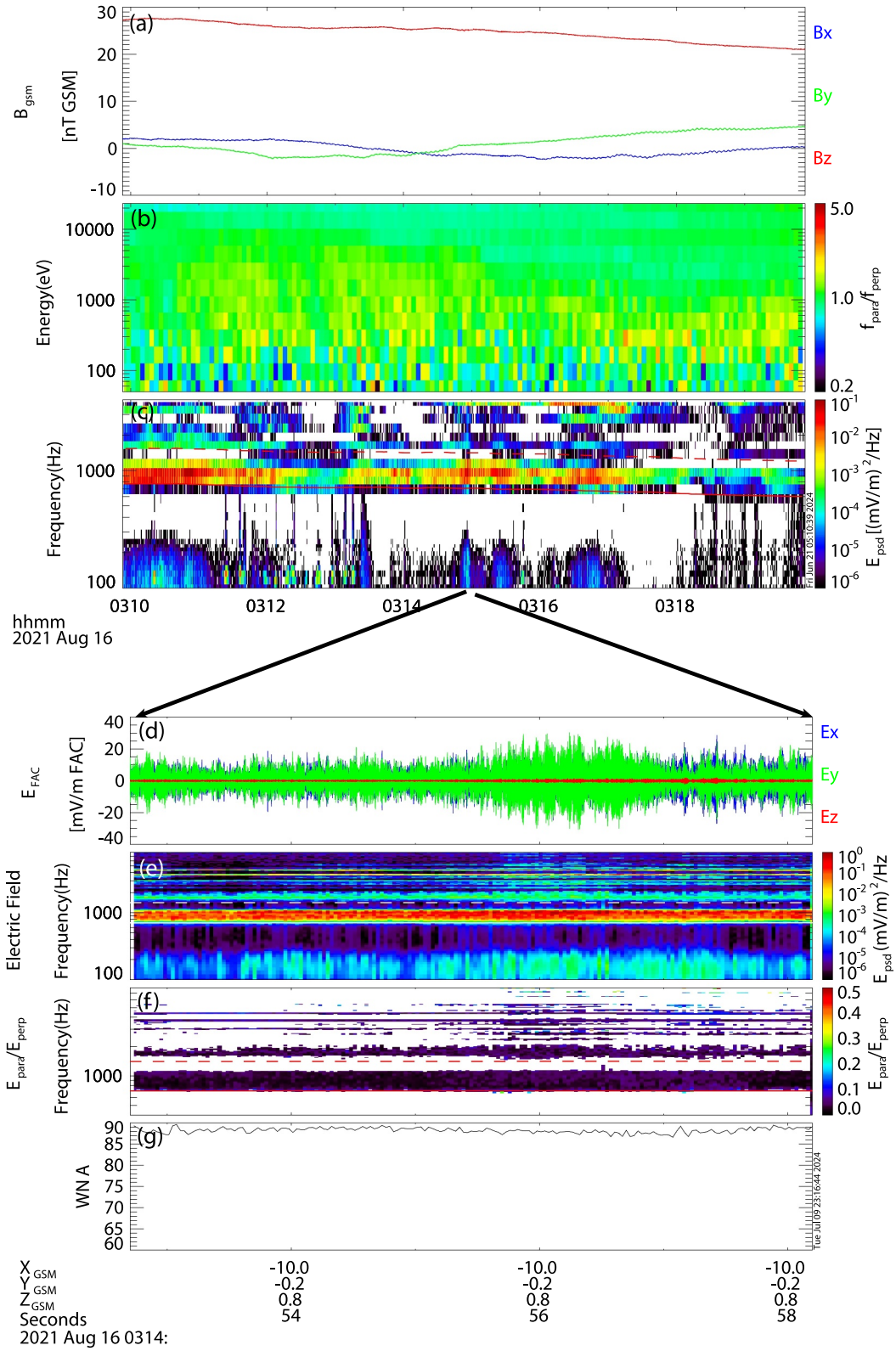

Figure 5.

precipitation. Beam-driven ECH waves can scatter low energy electron beams in the sub-keV energy range out of the loss cone, energize them, and subsequently trap them in the magnetosphere as discussed in Section 3. Loss-cone-driven ECH waves, however, barely interact with low-energy electrons at tens of eV. The difference in resonance energies of these two wave modes results primarily from their different wave normal angles. Beam-driven ECH waves propagate at moderately oblique wave normal angles, while loss-cone-driven ECH waves propagate at wave normal angles close to 90°. The resonance velocities at $N = 1$ and $N = 2$ for ECH waves are $v_{res,N=1} = (\omega - \Omega_{ce})/(k\cos\theta)$ and $v_{res,N=2} = (\omega - 2\Omega_{ce})/(k\cos\theta)$. Compared with loss-cone-driven ECH waves, $k_{\|} = k\cos\theta$ for beam-driven ECH waves is larger, and the resonance velocities at $N = 1$ and $N = 2$ are smaller. Therefore, beam-driven ECH waves can resonantly interact with low energy electrons, while loss-cone-driven ECH waves cannot.

5. Summary and Discussion

In our study, we modified the equations in Horne and Thorne (2000) to account for the propagation direction of ECH waves and calculate their diffusion coefficients. We investigated a typical beam-driven ECH event propagating at $\theta \sim 77°$ and calculated the bounce-averaged diffusion coefficients in pitch angle, momentum, and mixed terms. Our results demonstrate that beam-driven ECH waves can resonantly interact with low energy electron beams from tens of eV to a few hundred eV. These electron beams can be energized and scattered to larger pitch angles through Landau resonance and cyclotron resonances of order N =1 and 2. Beam-driven ECH waves can also drive the precipitation of plasma sheet electrons at higher energies from a few hundred eV to a few keV through higher order cyclotron resonances. That beam-driven ECH waves can energize and scatter electrons of tens of eV is in stark contrast to loss-cone-driven ECH waves (with $\theta \sim 89°$) which rarely interact with low energy electrons. The latter are mainly responsible for the scattering of plasma sheet electrons at a few hundred eV to a few keV (Belmont et al., 1983; Ni, Thorne, Horne, et al., 2011; Zhang et al., 2015). Such discrepancy in resonance energies mainly arises from different wave propagation direction affecting resonance velocities $v_{res} = (\omega - N\Omega_{ce})/(k\cos\theta)$. Apart from the wave normal angle, wave frequency also affects resonance velocities. While loss cone driven ECH waves close to f_{ce} or $2f_{ce}$ can also resonantly interact with low energy electron beams as discussed in Horne (2015), the waves are most frequently observed in the frequency range between $1.1 < f/f_{ce} < 1.9$ (Meredith et al., 2009; Ni et al., 2017). Therefore, beam-driven ECH waves are more effective in thermalizing and scattering low energy electron outflows than loss-cone-driven ECH waves. Another parameter that affects the resonance energy of ECH waves is wavelength. The wavelength of ECH waves can be obtained from the hot plasma dispersion relation, as previously described by Horne & Thorne (2000); Ni, Thorne, Horne, et al. (2011). This dispersion relation, however, heavily depends on the number density and temperature of the cold electron population (Zhang, Angelopoulos, Artemyev, & Zhang, 2021). Cold electrons at ~1 eV can not be accurately measured by spacecraft due to photoelectron emissions. Additionally, uncertainty in determining the wavelength of ECH waves could also arise from the lack of accurate spacecraft measurements of the free energy sources of ECH waves. Because the field-of-view of particle instruments is generally much larger compared to the size of the loss cone ($1° \sim 2°$) (Angelopoulos et al., 2008; McFadden et al., 2008), loss cone distribution of plasma sheet electrons that excites loss-cone-driven ECH waves or low energy electron outflows confined within the loss cone that excites beam-driven ECH waves can not be accurately measured. Fortunately, we can measure the wavelength of ECH waves directly, using the interferometry technique (Zhang et al., 2022a, 2022b). This method can help calculate the resonance energy of ECH waves more precisely and could improve the estimations of diffusion coefficients in future studies.

Our work emphasizes the importance of beam-driven ECH waves affecting the dynamics of magnetosphere-ionosphere coupling. Ionospheric electron outflows in the sub-keV energy range are confined within the loss

Figure 5. An event of loss-cone-driven ECH waves observed by THEMIS-E spacecraft in the plasma sheet. (a) Magnetic field in GSM coordinate system; (b) Ratio between the parallel electron phase space density and perpendicular electron phase space density as a function electron energy and time. Red indicates field-aligned flux anisotropy and blue is perpendicular flux anisotropy; (c) Electric field dynamic power spectrum. Solid red line is f_{ce} and dashed red line is $2f_{ce}$; (d) Electric field waveform data in field-aligned coordinate system after high-pass filtering above 100 Hz; (e) Electric field dynamic power spectrum. Solid white line is f_{ce} and dashed white line is $2f_{ce}$; (f) Square root of the ratio between the parallel electric field power spectral density and the perpendicular power spectral density. Solid red line is f_{ce} and dashed red line is $2f_{ce}$. Only data points when the total power spectral density is larger than $10^{-4}(mV/m)^2/Hz$ are plotted; (g) Wave normal angle of ECH waves.

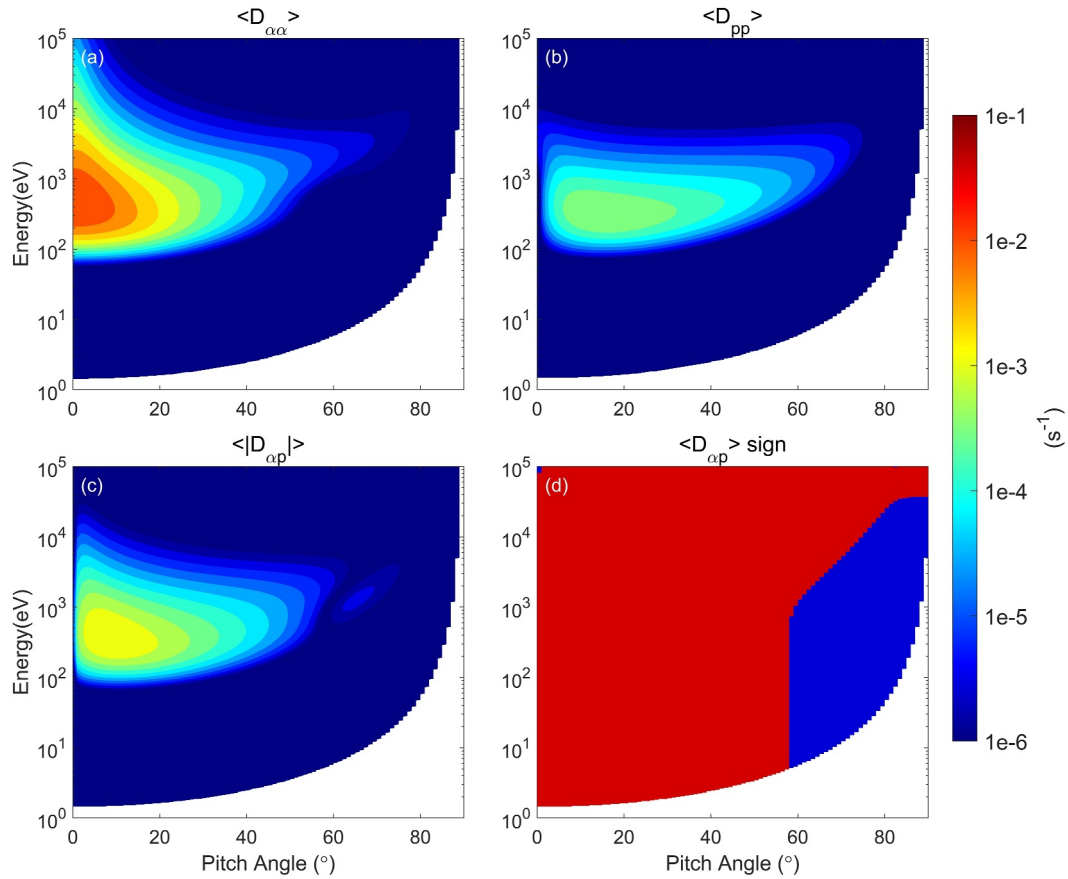

Figure 6. (a) Bounce-averaged pitch angle diffusion coefficient of loss-cone-driven ECH waves as a function of electron energy and electron pitch angle; (b) Bounce-averaged momentum diffusion coefficient; (c) Bounce-averaged mixed diffusion coefficient; (d) The sign of mixed diffusion coefficient. Red is positive sign and blue is negative sign.

cone of $1^\circ \sim 2^\circ$ when they reach the magnetic equator. These electron outflows can excite beam-driven ECH waves through Landau and cyclotron resonances. In turn, beam-driven ECH waves saturate by energizing and scattering electron beams (Zhang et al., 2024a, 2024b). Electron outflows can be scattered out of the loss cone through cyclotron resonance with beam-driven ECH waves. Once trapped in the magnetosphere, these electron beams can be observed by spacecraft instruments, which have a much wider field-of-view compared to the size of the loss cone. In fact, previous statistical studies demonstrate that there exists a field-aligned anisotropic electron population in sub-keV energies both in the inner magnetosphere and in the plasma sheet (Artemyev et al., 2014; Walsh et al., 2011). This sub-keV electron population, likely of ionospheric origin (Walsh et al., 2013; Wright et al., 2008; Zheng et al., 2012), is of potential importance to magnetospheric dynamics. Plasma sheet electrons are frequently observed to have a finite field-aligned temperature anisotropy around $T_{\parallel}/T_{\perp} \approx 1.1$ (Artemyev et al., 2013; Stiles et al., 1978) and this temperature anisotropy is provided by the sub-keV electron population. This field-aligned anisotropic electron population can significantly modify local currents in the magnetotail current sheet (Artemyev, Angelopoulos, et al., 2020; Kamaletdinov et al., 2020; Karimabadi et al., 2004). Additionally, the trapping of these low energy electron outflows in the magnetosphere can alter macroscopic plasma parameters, such as electron density (Khazanov et al., 2014). Electron density determines the electron plasma frequency ω_{pe} and ω_{pe}/ω_{ce} is a crucial parameter affecting the generation, saturation and propagation of almost all the electron-driven instabilities (Li et al., 2009; Li et al., 2016; An, Yue, et al., 2017; An, Bortnik, et al., 2017; Shi et al., 2023; D. Ma et al., 2024). Therefore, ECH-driven scattering and magnetic trapping of ionosphere outflows to the magnetosphere may provide a new channel for magnetosphere-ionosphere coupling, and modify the properties of electron-driven instabilities responsible for electromagnetic wave generation in the equatorial magnetosphere. Among these electron-driven instabilities, whistler-mode chorus waves can scatter energetic electrons into the ionosphere and also accelerate electrons to relativistic energy range (Li et al., 2014;

Thorne et al., 2010, 2013). Moreover, the trapping of electron outflows in the magnetosphere can increase the plasma density and consequently decrease the local Alfven velocity. This change in Alfven velocity could affect the energy transport from the magnetotail toward the inner magnetosphere and from the magnetosphere to the ionosphere (Angelopoulos et al., 2002; Keiling, 2009).

Evaluating diffusion coefficients of beam-driven and loss-cone-driven ECH waves is the first step toward a statistical quantification of the two different ECH wave modes on plasma sheet electron precipitation. Combining the statistical distribution on ECH waves and their properties, linear dispersion relations and the equations of quasi-linear diffusion coefficients, future studies should be able to systematically quantify diffuse aurora precipitation driven by these two ECH wave modes. Our present study aims to facilitate improved models of electron scattering and diffuse aurora precipitation resulting from ECH wave-particle interactions.

Data Availability Statement

THEMIS data used in this study are available at http://themis.ssl.berkeley.edu. Analysis on THEMIS data was done using Space Physics Environment Data Analysis Software (SPEDAS), available at https://spedas.org/. The simulation data have been archived on Zenodo (Zhang et al., 2024a, 2024b): at https://doi.org/10.5281/zenodo.13129613.

Acknowledgments
This work was supported from NASA grants 80NSSC22K1638, 80NSSC22K1634 and NASA contract NAS5-02099. Anton Artemyev and Xiaojia Zhang acknowledge support from 80NSSC23K0413, 80NSSC20K1325. Qianli Ma acknowledges supports from NASA grants 80NSSC20K0196 and 80NSSC24K0572, and NSF grant AGS-2225445. Xin An acknowledges support from NSF Grant 2108582. We acknowledge NASA contract NAS5-02099 for the use of data from the THEMIS mission. We thank J.W. Bonnell and F.S. Mozer for the use of EFI data; C. W. Carlson and J. P. McFadden for use of ESA data; A. Roux and O. Le Contel for use of SCM data; K. H. Glassmeier, U. Auster and W. Baumjohann for the use of FGM data provided under the lead of the Technical University of Braunschweig and with financial support through the German Ministry for Economy and Technology and the German Center for Aviation and Space (DLR) under contract 50 OC 0302. Data access and processing were done using SPEDAS V3.1, see Angelopoulos et al. (2019).

References

Abel, G. A., Fazakerley, A. N., & Johnstone, A. D. (2002a). Simultaneous acceleration and pitch angle scattering of field-aligned electrons observed by the LEPA on CRRES. *Journal of Geophysical Research (Space Physics)*, *107*(A12), 1416. https://doi.org/10.1029/2001JA005090

Abel, G. A., Fazakerley, A. N., & Johnstone, A. D. (2002b). Statistical distributions of field-aligned electron events in the near-equatorial magnetosphere observed by the Low Energy Plasma Analyzer on CRRES. *Journal of Geophysical Research*, *107*(A11), 1393. https://doi.org/10.1029/2001JA005073

Albert, J. M. (2007). Simple approximations of quasi-linear diffusion coefficients. *Journal of Geophysical Research*, *112*(A12), 12202. https://doi.org/10.1029/2007JA012551

An, X., Bortnik, J., Van Compernolle, B., Decyk, V., & Thorne, R. (2017a). Electrostatic and whistler instabilities excited by an electron beam. *Physics of Plasmas*, *24*(7), 072116. https://doi.org/10.1063/1.4986511

An, X., Bortnik, J., & Zhang, X.-J. (2021). Nonlinear Landau resonant interaction between Kinetic Alfvén waves and thermal electrons: Excitation of time domain structures. *Journal of Geophysical Research (Space Physics)*, *126*(1), e28643. https://doi.org/10.1029/2020JA028643

An, X., Yue, C., Bortnik, J., Decyk, V., Li, W., & Thorne, R. M. (2017b). On the parameter dependence of the whistler anisotropy instability. *Journal of Geophysical Research*, *122*(2), 2001–2009. https://doi.org/10.1002/2017JA023895

Angelopoulos, V. (2008). The THEMIS mission. *Space Science Reviews*, *141*(1–4), 5–34. https://doi.org/10.1007/s11214-008-9336-1

Angelopoulos, V. (2011). The ARTEMIS mission. *Space Science Reviews*, *165*(1–4), 3–25. https://doi.org/10.1007/s11214-010-9687-2

Angelopoulos, V., Baumjohann, W., Kennel, C. F., Coronti, F. V., Kivelson, M. G., Pellat, R., et al. (1992). Bursty bulk flows in the inner central plasma sheet. *Journal of Geophysical Research*, *97*(A4), 4027–4039. https://doi.org/10.1029/91JA02701

Angelopoulos, V., Chapman, J. A., Mozer, F. S., Scudder, J. D., Russell, C. T., Tsuruda, K., et al. (2002). Plasma sheet electromagnetic power generation and its dissipation along auroral field lines. *Journal of Geophysical Research*, *107*(A8), 1181. https://doi.org/10.1029/2001JA900136

Angelopoulos, V., Cruce, P., Drozdov, A., Grimes, E. W., Hatzigeorgiu, N., King, D. A., et al. (2019). The space physics environment data analysis system (SPEDAS). *Space Science Reviews*, *215*(1), 9. https://doi.org/10.1007/s11214-018-0576-4

Angelopoulos, V., Sibeck, D., Carlson, C. W., McFadden, J. P., Larson, D., Lin, R. P., et al. (2008). First results from the THEMIS mission. *Space Science Reviews*, *141*(1–4), 453–476. https://doi.org/10.1007/s11214-008-9378-4

Artemyev, A. V., Agapitov, O., Mourenas, D., Krasnoselskikh, V., Shastun, V., & Mozer, F. (2016). Oblique whistler-mode waves in the Earth's inner magnetosphere: Energy distribution, origins, and role in radiation belt dynamics. *Space Science Reviews*, *200*(1–4), 261–355. https://doi.org/10.1007/s11214-016-0252-5

Artemyev, A. V., Angelopoulos, V., Vasko, I. Y., Petrukovich, A. A., Runov, A., Saito, Y., et al. (2020a). Contribution of anisotropic electron current to the magnetotail current sheet as a function of location and plasma conditions. *Journal of Geophysical Research: Space Physics*, *125*(1), e2019JA027251. https://doi.org/10.1029/2019JA027251

Artemyev, A. V., Petrukovich, A. A., Nakamura, R., & Zelenyi, L. M. (2013). Profiles of electron temperature and B_z along Earth's magneto tail. *Annales Geophysicae*, *31*(6), 1109–1114. https://doi.org/10.5194/angeo-31-1109-2013

Artemyev, A. V., Walsh, A. P., Petrukovich, A. A., Baumjohann, W., Nakamura, R., & Fazakerley, A. N. (2014). Electron pitch angle/energy distribution in the magneto tail. *Journal of Geophysical Research*, *119*(9), 7214–7227. https://doi.org/10.1002/2014JA020350

Artemyev, A. V., Zhang, X. J., Angelopoulos, V., Mourenas, D., Vainchtein, D., Shen, Y., et al. (2020b). Ionosphere feedback to electron scattering by equatorial whistler mode waves. *Journal of Geophysical Research (Space Physics)*, *125*(9), e28373. https://doi.org/10.1029/2020JA028373

Ashour-Abdalla, M., & Kennel, C. F. (1978). Nonconvective and convective electron cyclotron harmonic instabilities. *Journal of Geophysical Research*, *83*(A4), 1531–1543. https://doi.org/10.1029/JA083iA04p01531

Ashour-Abdalla, M., Kennel, C. F., & Livesey, W. (1979). A parametric study of electron multi harmonic instabilities in the magnetosphere. *Journal of Geophysical Research*, *84*(A11), 6540–6546. https://doi.org/10.1029/JA084iA11p06540

Auster, H. U., Glassmeier, K. H., Magnes, W., Aydogar, O., Baumjohann, W., Constantinescu, D., et al. (2008). The THEMIS fluxgate magnetometer. *Space Science Reviews*, *141*(1–4), 235–264. https://doi.org/10.1007/s11214-008-9365-9

Belmont, G., Fontaine, D., & Canu, P. (1983). Are equatorial electron cyclotron waves responsible for diffuse auroral electron precipitation? *Journal of Geophysical Research*, *88*(A11), 9163–9170. https://doi.org/10.1029/JA088iA11p09163

Bonnell, J. W., Mozer, F. S., Delory, G. T., Hull, A. J., Ergun, R. E., Cully, C. M., et al. (2008). The electric field instrument (EFI) for THEMIS. *Space Science Reviews*, *141*(1–4), 303–341. https://doi.org/10.1007/s11214-008-9469-2

Carlson, C. W., McFadden, J. P., Ergun, R. E., Temerin, M., Peria, W., Mozer, F. S., et al. (1998). FAST observations in the downward auroral current region: Energetic upgoing electron beams, parallel potential drops, and ion heating. *Geophysical Research Letters*, *25*(12), 2017–2020. https://doi.org/10.1029/98GL00851

Cattell, C., Dombeck, J., Yusof, W., Carlson, C., & McFadden, J. (2004). Fast observations of the solar illumination dependence of upflowing electron beams in the auroral zone. *Journal of Geophysical Research*, *109*(A2). https://doi.org/10.1029/2003JA010075

Chappell, C. R., Huddleston, M. M., Moore, T. E., Giles, B. L., & Delcourt, D. C. (2008). Observations of the warm plasma cloak and an explanation of its formation in the magnetosphere. *Journal of Geophysical Research (Space Physics)*, *113*(A9), A09206. https://doi.org/10.1029/2007JA012945

Cully, C. M., Ergun, R. E., Stevens, K., Nammari, A., & Westfall, J. (2008). The THEMIS digital fields board. *Space Science Reviews*, *141*(1–4), 343–355. https://doi.org/10.1007/s11214-008-9417-1

Denton, M. H., Reeves, G. D., Larsen, B. A., Friedel, R. F. W., Thomsen, M. F., Fernandes, P. A., et al. (2017). On the origin of low-energy electrons in the inner magnetosphere: Fluxes and pitch-angle distributions. *Journal of Geophysical Research (Space Physics)*, *122*(2), 1789–1802. https://doi.org/10.1002/2016JA023648

Elphic, R. C., Bonnell, J., Strangeway, R. J., Carlson, C. W., Temerin, M., McFadden, J. P., et al. (2000). Fast observations of upward accelerated electron beams and the downward field-aligned current region. In *Magnetospheric Current Systems* (pp. 173–180). American Geophysical Union (AGU). https://doi.org/10.1029/GM118p0173

Ergun, R. E., Carlson, C. W., McFadden, J. P., Mozer, F. S., Delory, G. T., Peria, W., et al. (1998). FAST satellite observations of large-amplitude solitary structures. *Geophysical Research Letters*, *25*(12), 2041–2044. https://doi.org/10.1029/98GL00636

Ergun, R. E., Su, Y. J., Andersson, L., Carlson, C. W., McFadden, J. P., Mozer, F. S., et al. (2001). Direct observation of localized parallel electric fields in a space plasma. *Physical Review Letters*, *87*(4), 045003. https://doi.org/10.1103/PhysRevLett.87.045003

Fontaine, D., & Blanc, M. (1983). A theoretical approach to the morphology and the dynamics of diffuse auroral zones. *Journal of Geophysical Research*, *88*(A9), 7171–7184. https://doi.org/10.1029/JA088iA09p07171

Frank, L. A., & Ackerson, K. L. (1971). Observations of charged particle precipitation into the auroral zone. *Journal of Geophysical Research*, *76*(16), 3612–3643. https://doi.org/10.1029/JA076i016p03612

Fredricks, R. W. (1971). Plasma instability at (n + ½) f_c and its relationship to some satellite observations. *Journal of Geophysical Research*, *76*(22), 5344–5348. https://doi.org/10.1029/JA076i022p05344

Fredricks, R. W., & Scarf, F. L. (1973). Recent studies of magnetospheric electric field emissions above the electron gyro frequency. *Journal of Geophysical Research*, *78*(1), 310–314. https://doi.org/10.1029/JA078i001p00310

Glauert, S. A., & Horne, R. B. (2005). Calculation of pitch angle and energy diffusion coefficients with the PADIE code. *Journal of Geophysical Research*, *110*(A4), 4206. https://doi.org/10.1029/2004JA010851

Gough, M. P., Christiansen, P. J., Martelli, G., & Gershuny, E. J. (1979). Interaction of electrostatic waves with warm electrons at the geomagnetic equator. *Nature*, *279*(5713), 515–517. https://doi.org/10.1038/279515a0

Horne, R. B. (1989). Path-integrated growth of electrostatic waves - the generation of terrestrial myriametric radiation. *Journal of Geophysical Research*, *94*(A7), 8895–8909. https://doi.org/10.1029/JA094iA07p08895

Horne, R. B. (2015). Trapping and acceleration of upflowing ionospheric electrons in the magnetosphere by electrostatic electron cyclotron harmonic waves. *Geophysical Research Letters*, *42*(4), 975–980. https://doi.org/10.1002/2014GL062406

Horne, R. B., & Thorne, R. M. (2000). Electron pitch angle diffusion by electrostatic electron cyclotron harmonic waves: The origin of pancake distributions. *Journal of Geophysical Research*, *105*(A3), 5391–5402. https://doi.org/10.1029/1999JA900447

Horne, R. B., Thorne, R. M., Meredith, N. P., & Anderson, R. R. (2003). Diffuse auroral electron scattering by electron cyclotron harmonic and whistler mode waves during an isolated substorm. *Journal of Geophysical Research*, *108*(A7), 1290. https://doi.org/10.1029/2002JA009736

Iijima, T., & Potemra, T. A. (1976). The amplitude distribution of field-aligned currents at northern high latitudes observed by triad. *Journal of Geophysical Research (1896-1977)*, *81*(13), 2165–2174. https://doi.org/10.1029/JA081i013p02165

Iijima, T., & Potemra, T. A. (1978). Large-scale characteristics of field-aligned currents associated with substorms. *Journal of Geophysical Research*, *83*(A2), 599–615. https://doi.org/10.1029/JA083iA02p00599

Kamaletdinov, S. R., Yushkov, E. V., Artemyev, A. V., Lukin, A. S., & Vasko, I. Y. (2020). Superthin current sheets supported by anisotropic electrons. *Physics of Plasmas*, *27*(8), 082904. https://doi.org/10.1063/5.0018063

Karimabadi, H., Daughton, W., & Quest, K. B. (2004). Role of electron temperature anisotropy in the onset of magnetic reconnection. *Geophysical Research Letters*, *31*(18), 18801. https://doi.org/10.1029/2004GL020791

Karpman, V. I., Alekhin, I. K., Borisov, N. D., & Riabova, N. A. (1975). Electrostatic electron-cyclotron waves in plasma with a loss-cone distribution. *Plasma Physics*, *17*(5), 361–372. https://doi.org/10.1088/0032-1028/17/5/006

Keiling, A. (2009). Alfvén waves and their roles in the dynamics of the Earth's magnetotail: A review. *Space Science Reviews*, *142*(1–4), 73–156. https://doi.org/10.1007/s11214-008-9463-8

Kennel, C. F., & Petschek, H. E. (1966). Limit on stably trapped particle fluxes. *Journal of Geophysical Research*, *71*, 1–28. https://doi.org/10.1029/jz071i001p00001

Kennel, C. F., Scarf, F. L., Fredricks, R. W., McGehee, J. H., & Coroniti, F. V. (1970). VLF electric field observations in the magnetosphere. *Journal of Geophysical Research*, *75*(31), 6136–6152. https://doi.org/10.1029/JA075i031p06136

Khazanov, G. V., Chen, M. W., Lemon, C. L., & Sibeck, D. G. (2019). The magnetosphere-ionosphere electron precipitation dynamics and their geospace consequences during the 17 March 2013 storm. *Journal of Geophysical Research (Space Physics)*, *124*(8), 6504–6523. https://doi.org/10.1029/2019JA026589

Khazanov, G. V., Glocer, A., & Himwich, E. W. (2014). Magnetosphere-ionosphere energy interchange in the electron diffuse aurora. *Journal of Geophysical Research (Space Physics)*, *119*(1), 171–184. https://doi.org/10.1002/2013JA019325

Khazanov, G. V., Sibeck, D. G., & Zesta, E. (2017). Major pathways to electron distribution function formation in regions of diffuse aurora. *Journal of Geophysical Research (Space Physics)*, *122*(4), 4251–4265. https://doi.org/10.1002/2017JA023956

Li, W., Mourenas, D., Artemyev, A. V., Bortnik, J., Thorne, R. M., Kletzing, C. A., et al. (2016). Unraveling the excitation mechanisms of highly oblique lower band chorus waves. *Geophysical Research Letters*, *43*(17), 8867–8875. https://doi.org/10.1002/2016GL070386

Li, W., Thorne, R. M., Angelopoulos, V., Bonnell, J. W., McFadden, J. P., Carlson, C. W., et al. (2009). Evaluation of whistler-mode chorus intensification on the night side during an injection event observed on the THEMIS spacecraft. *Journal of Geophysical Research*, *114*(A1), 0. https://doi.org/10.1029/2008JA013554

Li, W., Thorne, R. M., Ma, Q., Ni, B., Bortnik, J., Baker, D. N., et al. (2014). Radiation belt electron acceleration by chorus waves during the 17 March 2013 storm. *Journal of Geophysical Research*, *119*(6), 4681–4693. https://doi.org/10.1002/2014JA019945

Liang, J., Ni, B., Spanswick, E., Kubyshkina, M., Donovan, E. F., Uritsky, V. M., et al. (2011). Fast earthward flows, electron cyclotron harmonic waves, and diffuse auroras: Conjunctive observations and a synthesized scenario. *Journal of Geophysical Research (Space Physics)*, *116*(A12), A12220. https://doi.org/10.1029/2011JA017094

Liu, J., Angelopoulos, V., Runov, A., & Zhou, X.-Z. (2013a). On the current sheets surrounding dipolarizing flux bundles in the magnetotail: The case for wedgelets. *Journal of Geophysical Research*, *118*(5), 2000–2020. https://doi.org/10.1002/jgra.50092

Liu, J., Angelopoulos, V., Zhou, X.-Z., Runov, A., & Yao, Z. (2013b). On the role of pressure and flow perturbations around dipolarizing flux bundles. *Journal of Geophysical Research*, *118*(11), 7104–7118. https://doi.org/10.1002/2013JA019256

Liu, X., Chen, L., Gu, W., & Zhang, X.-J. (2018). Electron cyclotron harmonic wave instability by loss cone distribution. *Journal of Geophysical Research (Space Physics)*, *123*(11), 9035–9044. https://doi.org/10.1029/2018JA025925

Lou, Y., Gu, X., Summers, D., Ni, B., Liu, K., Fu, S., et al. (2018). Statistical distributions of dayside ECH waves observed by MMS. *Geophysical Research Letters*, *45*(23), 12730–12738. https://doi.org/10.1029/2018GL080125

Lyons, L. R. (1974). Electron diffusion driven by magnetospheric electrostatic waves. *Journal of Geophysical Research*, *79*(4), 575–580. https://doi.org/10.1029/JA079i004p00575

Lyons, L. R. (1984). Electron energization in the geomagnetic tail current sheet. *Journal of Geophysical Research*, *89*(A7), 5479–5487. https://doi.org/10.1029/JA089iA07p05479

Lysak, R. L. (1990). Electrodynamic coupling of the magnetosphere and ionosphere. *Space Science Reviews*, *52*(1–2), 33–87. https://doi.org/10.1007/BF00704239

Ma, D., An, X., Artemyev, A., Bortnik, J., Angelopoulos, V., & Zhang, X.-J. (2024). Nonlinear Landau resonant interaction between whistler waves and electrons: Excitation of electron-acoustic waves. *Physics of Plasmas*, *31*(2), 022304. https://doi.org/10.1063/5.0171227

Ma, Q., Li, W., Thorne, R. M., Nishimura, Y., Zhang, X.-J., Reeves, G. D., et al. (2016). Simulation of energy-dependent electron diffusion processes in the Earth's outer radiation belt. *Journal of Geophysical Research*, *121*(5), 4217–4231. https://doi.org/10.1002/2016JA022507

Ma, Q., Ni, B., Tao, X., & Thorne, R. M. (2012). Evolution of the plasma sheet electron pitch angle distribution by whistler-mode chorus waves in non-dipole magnetic fields. *Annales Geophysicae*, *30*(4), 751–760. https://doi.org/10.5194/angeo-30-751-2012

Marshall, R. A., & Bortnik, J. (2018). Pitch angle dependence of energetic electron precipitation: Energy deposition, backscatter, and the bounce loss cone. *Journal of Geophysical Research (Space Physics)*, *123*(3), 2412–2423. https://doi.org/10.1002/2017JA024873

McFadden, J. P., Carlson, C. W., Larson, D., Ludlam, M., Abiad, R., Elliott, B., et al. (2008). The THEMIS ESA plasma instrument and in-flight calibration. *Space Science Reviews*, *141*(1–4), 277–302. https://doi.org/10.1007/s11214-008-9440-2

Meredith, N. P., Horne, R. B., Thorne, R. M., & Anderson, R. R. (2009). Survey of upper band chorus and ECH waves: Implications for the diffuse aurora. *Journal of Geophysical Research (Space Physics)*, *114*(A7), A07218. https://doi.org/10.1029/2009JA014230

Mourenas, D., Artemyev, A. V., Ripoll, J.-F., Agapitov, O. V., & Krasnoselskikh, V. V. (2012). Timescales for electron quasi-linear diffusion by parallel and oblique lower-band Chorus waves. *Journal of Geophysical Research*, *117*(A6), A06234. https://doi.org/10.1029/2012JA017717

Mourenas, D., Artemyev, A. V., Zhang, X. J., Angelopoulos, V., Tsai, E., & Wilkins, C. (2021). Electron lifetimes and diffusion rates inferred from ELFIN measurements at low altitude: First results. *Journal of Geophysical Research (Space Physics)*, *126*(11), e29757. https://doi.org/10.1029/2021JA029757

Mozer, F. S., Carlson, C. W., Hudson, M. K., Torbert, R. B., Parady, B., Yatteau, J., & Kelley, M. C. (1977). Observations of paired electrostatic shocks in the polar magnetosphere. *Physical Review Letters*, *38*(6), 292–295. https://doi.org/10.1103/PhysRevLett.38.292

Nakamura, R., Baumjohann, W., Klecker, B., Bogdanova, Y., Balogh, A., Rème, H., et al. (2002). Motion of the dipolarization front during a flow burst event observed by Cluster. *Geophysical Research Letters*, *29*(20), 200000–200001. https://doi.org/10.1029/2002GL015763

Newell, P. T., Sotirelis, T., & Wing, S. (2009). Diffuse, monoenergetic, and broadband aurora: The global precipitation budget. *Journal of Geophysical Research*, *114*(A9), A09207. https://doi.org/10.1029/2009JA014326

Ni, B., Gu, X., Fu, S., Xiang, Z., & Lou, Y. (2017). A statistical survey of electrostatic electron cyclotron harmonic waves based on THEMIS FFF wave data. *Journal of Geophysical Research (Space Physics)*, *122*(3), 3342–3353. https://doi.org/10.1002/2016JA023433

Ni, B., Liang, J., Thorne, R. M., Angelopoulos, V., Horne, R. B., Kubyshkina, M., et al. (2012a). Efficient diffuse auroral electron scattering by electrostatic electron cyclotron harmonic waves in the outer magnetosphere: A detailed case study. *Journal of Geophysical Research*, *117*(A1), 1218. https://doi.org/10.1029/2011JA017095

Ni, B., Thorne, R., Liang, J., Angelopoulos, V., Cully, C., Li, W., et al. (2011a). Global distribution of electrostatic electron cyclotron harmonic waves observed on THEMIS. *Geophysical Research Letters*, *38*(17), L17105. https://doi.org/10.1029/2011GL048793

Ni, B., Thorne, R. M., Horne, R. B., Meredith, N. P., Shprits, Y. Y., Chen, L., & Li, W. (2011b). Resonant scattering of plasma sheet electrons leading to diffuse auroral precipitation: 1. Evaluation for electrostatic electron cyclotron harmonic waves. *Journal of Geophysical Research*, *116*(A4), 4218. https://doi.org/10.1029/2010JA016232

Ni, B., Thorne, R. M., & Ma, Q. (2012b). Bounce-averaged Fokker-Planck diffusion equation in non-dipolar magnetic fields with applications to the Dungey magnetosphere. *Annales Geophysicae*, *30*(4), 733–750. https://doi.org/10.5194/angeo-30-733-2012

Ni, B., Thorne, R. M., Shprits, Y. Y., & Bortnik, J. (2008). Resonant scattering of plasma sheet electrons by whistler-mode chorus: Contribution to diffuse auroral precipitation. *Geophysical Research Letters*, *35*(11), 11106. https://doi.org/10.1029/2008GL034032

Ni, B., Thorne, R. M., Zhang, X., Bortnik, J., Pu, Z., Xie, L., et al. (2016). Origins of the Earth's diffuse auroral precipitation. *Space Science Reviews*, *200*(1–4), 205–259. https://doi.org/10.1007/s11214-016-0234-7

Paranicas, C., Hughes, W. J., Singer, H. J., & Anderson, R. R. (1992). Banded electrostatic emissions observed by the CRRES plasma wave experiment. *Journal of Geophysical Research*, *97*(A9), 13889–13898. https://doi.org/10.1029/92JA01137

Roeder, J. L., & Koons, H. C. (1989). A survey of electron cyclotron waves in the magnetosphere and the diffuse auroral electron precipitation. *Journal of Geophysical Research*, *94*(A3), 2529–2541. https://doi.org/10.1029/JA094iA03p02529

Roux, A., Le Contel, O., Coillot, C., Bouabdellah, A., de La Porte, B., Alison, D., et al. (2008). The search coil magnetometer for THEMIS. *Space Science Reviews*, *141*(1–4), 265–275. https://doi.org/10.1007/s11214-008-9455-8

Runov, A., Angelopoulos, V., Sitnov, M. I., Sergeev, V. A., Bonnell, J., McFadden, J. P., et al. (2009). THEMIS observations of an earthward-propagating dipolarization front. *Geophysical Research Letters*, *36*(14), L14106. https://doi.org/10.1029/2009GL038980

Schulz, M., & Lanzerotti, L. J. (1974). *Particle diffusion in the radiation belts*. Springer.

Shen, Y., Artemyev, A., Zhang, X.-J., Vasko, I. Y., Runov, A., Angelopoulos, V., & Knudsen, D. (2020). Potential evidence of low-energy electron scattering and ionospheric precipitation by time domain structures. *Geophysical Research Letters*, *47*(16), e89138. https://doi.org/10.1029/2020GL089138

Shen, Y., Vasko, I. Y., Artemyev, A., Malaspina, D. M., Chu, X., Angelopoulos, V., & Zhang, X.-J. (2021). Realistic electron diffusion rates and lifetimes due to scattering by electron holes. *Journal of Geophysical Research (Space Physics)*, *126*(9), e29380. https://doi.org/10.1029/2021JA029380

Shi, X., Liu, T., Artemyev, A., Angelopoulos, V., Zhang, X.-J., & Turner, D. L. (2023). Intense whistler-mode waves at foreshock transients: Characteristics and regimes of wave-particle resonant interaction. *The Astrophysical Journal*, *944*(2), 193. https://doi.org/10.3847/1538-4357/acb543

Sibeck, D. G., & Angelopoulos, V. (2008). THEMIS science objectives and mission phases. *Space Science Reviews*, *141*(1–4), 35–59. https://doi.org/10.1007/s11214-008-9393-5

Stiles, G. S., Hones, E. W., Jr., Bame, S. J., & Asbridge, J. R. (1978). Plasma sheet pressure anisotropies. *Journal of Geophysical Research*, *83*(A7), 3166–3172. https://doi.org/10.1029/JA083iA07p03166

Strangeway, R. J., Ergun, R. E., Su, Y. J., Carlson, C. W., & Elphic, R. C. (2005). Factors controlling ionospheric outflows as observed at intermediate altitudes. *Journal of Geophysical Research (Space Physics)*, *110*(A3), A03221. https://doi.org/10.1029/2004JA010829

Summers, D., Ni, B., & Meredith, N. P. (2007). Timescales for radiation belt electron acceleration and loss due to resonant wave-particle interactions: 1. *Theory Journal of Geophysical Research*, *112*(A4), 4206. https://doi.org/10.1029/2006JA011801

Tao, X., Thorne, R. M., Li, W., Ni, B., Meredith, N. P., & Horne, R. B. (2011). Evolution of electron pitch angle distributions following injection from the plasma sheet. *Journal of Geophysical Research*, *116*(A4), A04229. https://doi.org/10.1029/2010JA016245

Thorne, R. M., Li, W., Ni, B., Ma, Q., Bortnik, J., Chen, L., et al. (2013). Rapid local acceleration of relativistic radiation-belt electrons by magnetospheric chorus. *Nature*, *504*(7480), 411–414. https://doi.org/10.1038/nature12889

Thorne, R. M., Ni, B., Tao, X., Horne, R. B., & Meredith, N. P. (2010). Scattering by chorus waves as the dominant cause of diffuse auroral precipitation. *Nature*, *467*(7318), 943–946. https://doi.org/10.1038/nature09467

Tsyganenko, N. A. (1995). Modeling the Earth's magnetospheric magnetic field confined within a realistic magnetopause. *Journal of Geophysical Research*, *100*(A4), 5599–5612. https://doi.org/10.1029/94JA03193

Vasko, I. Y., Agapitov, O. V., Mozer, F. S., Artemyev, A. V., Krasnoselskikh, V. V., & Bonnell, J. W. (2017). Diffusive scattering of electrons by electron holes around injection fronts. *Journal of Geophysical Research*, *122*(3), 3163–3182. https://doi.org/10.1002/2016JA023337

Walsh, A. P., Fazakerley, A. N., Forsyth, C., Owen, C. J., Taylor, M. G. G. T., & Rae, I. J. (2013). Sources of electron pitch angle anisotropy in the magnetotail plasma sheet. *Journal of Geophysical Research*, *118*(10), 6042–6054. https://doi.org/10.1002/jgra.50553

Walsh, A. P., Owen, C. J., Fazakerley, A. N., Forsyth, C., & Dandouras, I. (2011). Average magnetotail electron and proton pitch angle distributions from Cluster PEACE and CIS observations. *Geophysical Research Letters*, *38*(6), 6103. https://doi.org/10.1029/2011GL046770

Wright, A. N., Owen, C. J., Chaston, C. C., & Dunlop, M. W. (2008). Downward current electron beam observed by Cluster and FAST. *Journal of Geophysical Research (Space Physics)*, *113*(A6), A06202. https://doi.org/10.1029/2007JA012643

Xiao, F., Su, Z., Zheng, H., & Wang, S. (2009). Modeling of outer radiation belt electrons by multidimensional diffusion process. *Journal of Geophysical Research*, *114*(A3), 3201. https://doi.org/10.1029/2008JA013580

Young, T. S. T., Callen, J. D., & McCune, J. E. (1973). High-frequency electrostatic waves in the magnetosphere. *Journal of Geophysical Research*, *78*(7), 1082–1099. https://doi.org/10.1029/JA078i007p01082

Yu, J., Wang, J., Chen, Z., Ren, A., Liu, X., Liu, N., et al. (2024). Statistical distribution of the peak frequency of ECH waves in the outer magnetosphere from magnetospheric multiscale satellite observations. *Journal of Geophysical Research (Space Physics)*, *129*(8), e2024JA032995. https://doi.org/10.1029/2024JA032995

Yu, J., Wang, J., Chen, Z., Ren, A., Liu, X., Liu, N., et al. (2023). Statistical evidence for off-equatorial minimum-B-pocket as a source region of electron cyclotron harmonic waves in the dayside outer magnetosphere. *Geophysical Research Letters*, *50*(14), e2022GL102583. https://doi.org/10.1029/2022GL102583

Zhang, X., An, X., Angelopoulos, V., Artemyev, A., Zhang, X.-J., & Jia, Y.-D. (2024a). Beam-driven electron cyclotron harmonic and electron acoustic waves as seen in particle-in-cell simulations. *Journal of Geophysical Research (Space Physics)*, *129*(6), e2023JA031851. https://doi.org/10.1029/2023JA031851

Zhang, X., Angelopoulos, V., Artemyev, A. V., & Liu, J. (2018). Whistler and electron firehose instability control of electron distributions in and around dipolarizing flux bundles. *Geophysical Research Letters*, *45*(18), 9380–9389. https://doi.org/10.1029/2018GL079613

Zhang, X., Angelopoulos, V., Artemyev, A. V., & Zhang, X.-J. (2021a). Beam-driven ECH waves: A parametric study. *Physics of Plasmas*, *28*(7), 072902. https://doi.org/10.1063/5.0053187

Zhang, X., Angelopoulos, V., Artemyev, A. V., Zhang, X.-J., An, X., & Liu, J. (2022a). Wavelength measurements of electron cyclotron harmonic waves in Earth's magnetotail. *Journal of Geophysical Research (Space Physics)*, *127*(7), e30500. https://doi.org/10.1029/2022JA030500

Zhang, X., Angelopoulos, V., Artemyev, A. V., Zhang, X.-J., & Liu, J. (2021b). Beam driven electron cyclotron harmonic waves in Earth's magnetotail. *Journal of Geophysical Research (Space Physics)*, *126*(3), e28743. https://doi.org/10.1029/2020JA028743

Zhang, X., Artemyev, A., Angelopoulos, V., Zhang, X., Ma, Q., An, X., & Jia, Y. (2024b). Resonant scattering of sub-keV electrons by beam-driven electron cyclotron harmonic waves [Dataset]. *Zenodo*. https://doi.org/10.5281/zenodo.13129613

Zhang, X.-J., & Angelopoulos, V. (2014). On the relationship of electrostatic cyclotron harmonic emissions with electron injections and dipolarization fronts. *Journal of Geophysical Research*, *119*(4), 2536–2549. https://doi.org/10.1002/2013JA019540

Zhang, X.-J., Angelopoulos, V., Ni, B., & Thorne, R. M. (2015). Predominance of ECH wave contribution to diffuse aurora in Earth's outer magnetosphere. *Journal of Geophysical Research*, *120*(1), 295–309. https://doi.org/10.1002/2014JA020455

Zhang, X.-J., Angelopoulos, V., Ni, B., Thorne, R. M., & Horne, R. B. (2013). Quasi-steady, marginally unstable electron cyclotron harmonic wave amplitudes. *Journal of Geophysical Research*, *118*(6), 3165–3172. https://doi.org/10.1002/jgra.50319

Zhang, X.-J., Angelopoulos, V., Ni, B., Thorne, R. M., & Horne, R. B. (2014). Extent of ECH wave emissions in the Earth's magnetotail. *Journal of Geophysical Research*, *119*(7), 5561–5574. https://doi.org/10.1002/2014JA019931

Zhang, X.-J., Artemyev, A., Angelopoulos, V., Tsai, E., Wilkins, C., Kasahara, S., et al. (2022b). Superfast precipitation of energetic electrons in the radiation belts of the Earth. *Nature Communications*, *13*(1), 1611. https://doi.org/10.1038/s41467-022-29291-8

Zheng, H., Fu, S. Y., Zong, Q. G., Pu, Z. Y., Wang, Y. F., & Parks, G. K. (2012). Observations of ionospheric electron beams in the plasma sheet. *Physical Review Letters*, *109*(20), 205001. https://doi.org/10.1103/PhysRevLett.109.205001